Carrier Photogeneration During UV-Vis Irradiation on Horizontal and Vertical Metal-Semiconductor Structures Based on Rutile-Phase TiO_2 Nanoparticles

Joel Molina, Carlos Zuniga, Edmundo Gutierrez
Electronics Department,
National Institute of Astrophysics, Optics and Electronics
Santa Maria Tonantzintla, Puebla, Mexico
E-mails: jmolina@inaoep.mx, czuniga@inaoep.mx, edmundo@inaoep.mx

Eunice Mendoza, Jose Luis Sanchez, Erick R. Bandala
Energy and Environment Research Group,
Universidad de las Americas, Puebla
San Andres Cholula, Puebla, Mexico
E-mails: edith.mendozaco@udlap.mx, jluis.sanchez@udlap.mx, erick.bandala@udlap.mx

***Abstract*—In this work, rutile-phase TiO_2 nanoparticles (np-TiO_2) are embedded within a Spin-On Glass oxide matrix (using a simple and economic Sol-Gel method) and the final TiO_2/SiO_2 mixture is directly deposited on stripes of aluminum so that the electronic, physical, chemical and photocatalytic characteristics of the final dielectric structure are obtained and correlated when irradiated with UV-Vis light sources. The I-V characteristics of this simple structure present a reduction in its total resistance when irradiated with UV light (compared to dark conditions), thus revealing a very simple photoresistor with relatively-low quantum efficiency.**

Keywords-TiO_2; nanoparticles; photoresistor; UV light; photogeneration; sol-gel processing; metal-semiconductor.

I. INTRODUCTION

Even though rutile-phase TiO_2 is considered as a very inefficient material in terms of its photocatalytic activity (ability for carrier photogeneration) [1-2], the use and development of this semiconductor material is quite important since the synthesis of TiO_2 usually produces a rutile phase quite easily, with relatively low concentration of impurities and also, economically. On the other hand, the synthesis of anatase-phase TiO_2 is more complicated, usually involving complex chemistry and/or doping with some metal or non-metal elements in order to increase its photocatalytic activity when exposed to UV or visible irradiation [3-6]. Also, using TiO_2 nanoparticles instead of dense TiO_2 thin films is useful in order to increase the contact surface area so that a higher density of photogenerated carriers is expected.

In this work, we embed rutile-phase TiO_2 nanoparticles (np-TiO_2) within an organic SiO_2 matrix and the final mixture of this dielectric structure is deposited on a thin film of aluminum. The final "horizontal" metal-semiconductor structure is then electrically characterized under dark and light conditions (I-V-light) so that the total resistance of a simple aluminum stripe is measured and correlated before and after UV irradiation. Compared to dark conditions, excess carriers are photogenerated within the TiO_2 nanoparticles after light exposure and they are directly transferred to both ends of the aluminum stripe after applying a low potential difference. The highest density of photogenerated carriers is obtained when the $TiO_2/SiO_2/Al$ is irradiated with UV-B light so that the total aluminum resistance is reduced by about 43%. Therefore, this initial device acts like a very simple "photoresistor". Additionally, we also fabricate so-called "vertical" metal-semiconductor-metal structures in order to obtain a solar energy conversion device with the intrinsic ability to self-store must of the converted energy in the form of a rechargeable capacitor. This device then acts like a very simple "photocapacitor" [7-8]. The *state-of-the-art* regarding these latest structures makes use of complex layered structures going from photo-rechargeable textiles for wearable power supplies [9], up to dye-sensitized solar cells (DSSC) connected in series with Li-ion batteries, metal oxides and/or TiO_2 nanotube arrays in order to increase energy conversion efficiency [10-12]. However, because of increasing fabrication complexity and use of a third additional electrode (in order to switch between the functions of energy conversion, storage and output) which consumes extra energy and increase cost of fabrication, a simpler two-electrode device is needed and that requirement is met by our proposed device structures.

This paper is arranged as follows: in Section I, we gave an introduction about the importance of testing simple "horizontal" and "vertical" metal-semiconductor structures which make use of TiO_2 nanoparticles in order to promote energy conversion in "photoresistor" and "photocapacitor" devices. Section II presents the experimental conditions used for fabrication of these structures as well as details about the measurement setup that is used for their physical and photo-electrical characterization. Section III presents and discusses the main experimental results that are found for these structures, thus confirming the ability of np-TiO_2 to act as photocatalytic material for both energy conversion and storage. Finally the main conclusions drawn from all results are highlighted in Section IV, from which we state that it is possible to use the "vertical" structure as a photocapacitor, thus enabling direct storage of solar energy.

II. EXPERIMENTAL

A. *Preparation of Thin FilmsBased on np-TiO_2*

We have used low-organic content or silicate-type spin-on glass (SOG)-based SiO_2 (700B from Filmtronics, Corp.) as a matrix for immobilization of np-TiO_2 (Dupont, R-706 with 93% purity and having an average diameter of 360 nm before embedding). Initially, specific amounts of commercial

 ISBN: 978-1-61208-297-4

np-TiO_2 are suspended in deionized water by hydrolyzing this TiO_2:H_2O mixture in a hot water bath (*baine marie*, 45°C, 30 min) and then, adding SOG-based SiO_2 so that the final TiO_2:SiO_2:H_2O mixture is again subjected to a final hot water bath (*baine marie*, 80°C, 1 hr) in order to obtain an homogeneous suspension. The concentration ratios of TiO_2 (solute) to SiO_2:H_2O (solvent) are 200, 100, 50 and 10 mg/mL and these solutions are labeled as A, B, C and D respectively. The solute concentrations were measured with an analytical balance AG285 from Mettler-Toledo. The final TiO_2:SiO_2:H_2O solutions were directly applied on the surface of clean glass slides (Corning glass 2947, size of 75 mm X 25mm), that were previously metalized with aluminum stripes, and sequentially spinned first at 3000 rpm, 30 sec, and then 4000 rpm, 15 sec in order to obtain uniform layers of np-TiO_2 embedded in SiO_2. After spinning, all films (A-D) were baked for 2 hours using a hot plate at 250°C in N_2 flow (99.99% purity) in order to evaporate mostly water and some of the organic solvents present in the SOG-based SiO_2 matrix. For FTIR characterization, the same processing sequence was followed and the final solution was applied on prime-grade P-type silicon wafers (100) with resistivity of 5–10 Ω·cm in order to eliminate most of the organic and impurity elements present within the Corning glass slides. In order to fabricate "vertical" structures, an additional ultra thin film layer of Titanium (100 Angstroms) is directly deposited atop the already described "horizontal" structures by E-beam evaporation under ultra high vacuum conditions (10^{-7} Torr) and with a very slow deposition rate of 1 Å/sec. Given the ultra low thermal budget required for fabrication of these simple structures, their introduction into large area flexible substrates is expected, thus promoting wide spread use of optimized devices. The fabrication process flows for both structures are briefly summarized, as shown in Fig. 1.

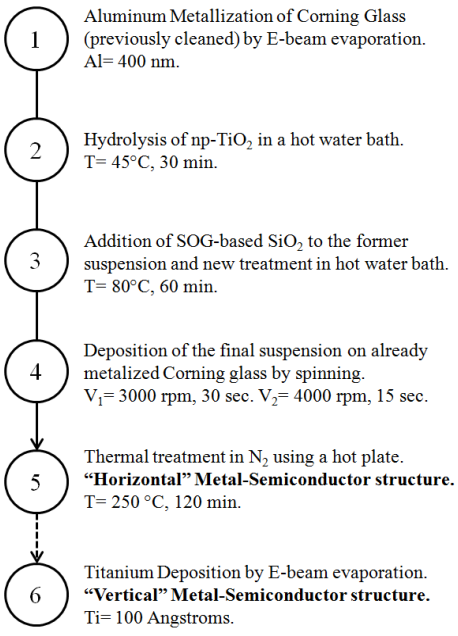

Figure 1. Process flow for fabrication of "horizontal" and "vertical" Metal-Semiconductor structures using np-TiO_2 as photoactive material.

It is important to notice that we did not chemically synthesize the np-TiO_2 used for fabrication of the proposed structures. Instead, we decided to use readily available commercial np-TiO_2 (with rather low purity of 93% and large average diameter of 360 nm) in order to test the ability of this material for carrier photogeneration under light irradiation.

B. Characterization of Materials and Aluminum-Stripes

DLS measurements (Nanotrac Wave, from Microtrac) [13] were done in order to determine the final size distribution of TiO_2 nanoparticles after the embedding process. By using DLS measurement technique, we are able to determine both the size and size distribution profile of TiO_2 nanoparticles in the final suspension before deposition on the glass surfaces. In particular, the size distribution profile for np-TiO_2 is obtained with high accuracy by this system (close to 100% signal intensity), thus giving a direct estimation of the homogeneity of the pn-TiO_2 in the final suspension. Also, thicknesses for all films were measured by profilometry (DEKTAK, V200-SI) after partially etching the TiO_2/SiO_2 film using a strong acid solution composed of diluted HF (HF:H_2O with 1:2 ratio). The crystalline phases of the resulting TiO_2-based films were obtained after XRD measurements using an X-ray diffractometer (Empyrean, from PANalytical), with a scanning step of 0.02°, using Cu-K_α radiation with λ= 1.5406 Å as an X-ray source. The band-gap energies Eg of the resulting films were calculated using optical transmittance data measured with an UV-Vis absorption spectrometer (LAMBDA 3B with double beam from Perkin Elmer, with Corning glass used as substrate) and the Tauc method [14]. Chemical compositional analyses for all films were obtained by FTIR spectrum measurements in absorbance mode with a Bruker Vector-22 system after 5 min of purge in N_2. The samples were measured against crystalline silicon substrate or SOG based silicon dioxide on glass (both were used as references). Finally, the I-V-light characteristics for the Al-stripes (covered with the TiO_2/SiO_2 structure) were obtained using an HP4156B semiconductor parameter analyzer at 300 K.

III. RESULTS AND DISCUSSION

A. Structure's Schematics and Energy Band Diagrams

Fig. 2 shows the 3-D and top view schematics for the first np-TiO_2/SiO_2 structure deposited on Aluminum/Glass. Because of the preparation method (previously discussed), we promote a uniform distribution of the np-TiO_2 within the oxide matrix so that these nanoparticles should have almost the same diameter size and separation in between as well. The aluminum stripes are 18X3 mm^2 in area with thickness of 400 nm. Fig. 3 shows the idealized energy-band diagrams for TiO_2 and TiO_2/SiO_2/Al systems during photogeneration of carriers after irradiation with energies $h\nu \geq Eg(TiO_2)$. In the first band diagram, all physical mechanisms during light irradiation, (1) excitation, (2) relaxation and (3) diffusion are also shown while a small potential difference is developed in the second diagram so that carriers are injected in the metal.

 ISBN: 978-1-61208-297-4

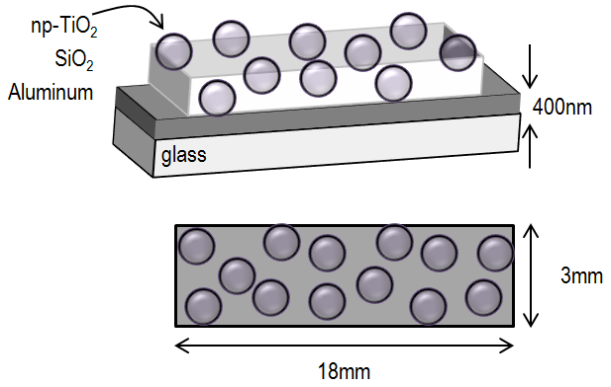

Figure 2. 3D and top views for np-TiO_2/SiO_2 deposited on Aluminum/Glass.

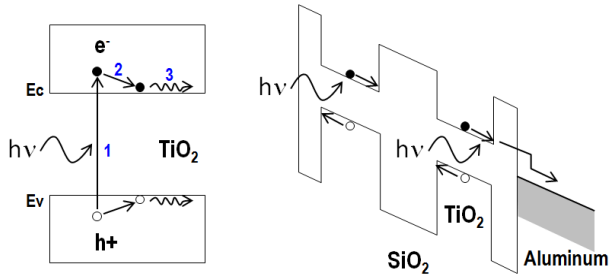

Figure 3. Idealized energy-band diagrams for TiO_2, TiO_2/SiO_2/Al systems.

B. *Dynamic Light Scattering (DLS) and Profilometry*

Fig. 4 shows the averaged particle size for TiO_2 before and after sonication. The dotted arrow shows the nominal average diameter as stated by the manufacturer ~360 nm.

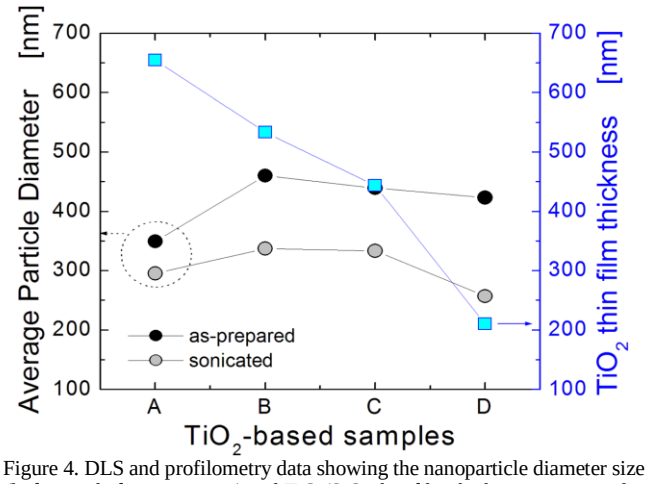

Figure 4. DLS and profilometry data showing the nanoparticle diameter size (before and after sonication) and TiO_2/SiO_2 thin film thickness respectively.

The as-prepared samples present larger particle diameter because of their tendency to agglomerate or aggregate after dispersion and settling within a liquid solution. During bath ultrasonication, dispersion of TiO_2 agglomerates is promoted by overcoming their weaker attractive forces, the final result being smaller np-TiO_2 diameters. The average physical size for sonicated np-TiO_2 is ~300 nm. Fig. 4 also shows the final np-TiO_2/SiO_2 film thickness after spinning deposition and thermal treatment of the prepared suspensions. We notice that thicker np-TiO_2/SiO_2 films are obtained for the more concentrated solutions as expected.

C. *X-Ray Diffraction (XRD)*

Fig. 5 shows the XRD diffraction patterns for all thin films including sample 0 (only SOG-based SiO_2 on glass).

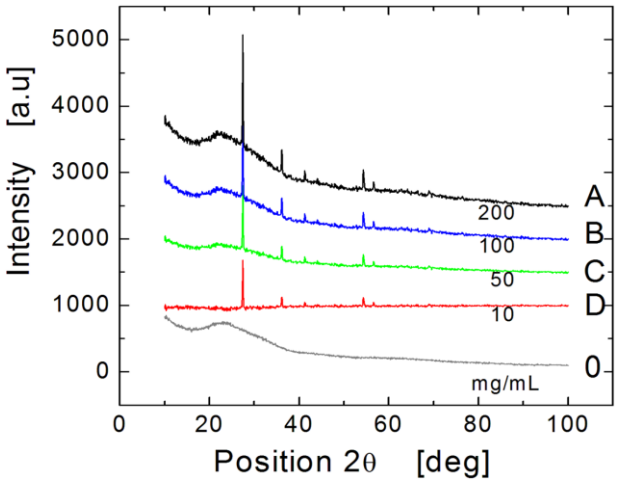

Figure 5. XRD data show existence of rutile phase for TiO_2 nanoparticles.

Samples A-B clearly present the characteristic sharp diffraction peaks for rutile phase TiO_2 including the broad amorphous phase from both the SiO_2 matrix and the glass slide (used for np-TiO_2 immobilization and as mechanical support respectively). Given the relatively high concentration density of np-TiO_2 embedded within the SiO_2 matrix for the A-B samples, it is clear that sharper diffraction peaks will be obtained possibly because of nanoparticles' agglomeration. This effect could be triggered during spinning, which make use of high speed centrifugal forces during step 4 of the process flow; see Fig. 1.

D. *Fourier-Transformed InfraRed (FTIR) Spectroscopy*

Fig. 6 shows typical chemical-bond vibration energies in absorption mode, found in samples A-D for all the range of interest (wavenumbers from 4000 down to 400 cm^{-1}).

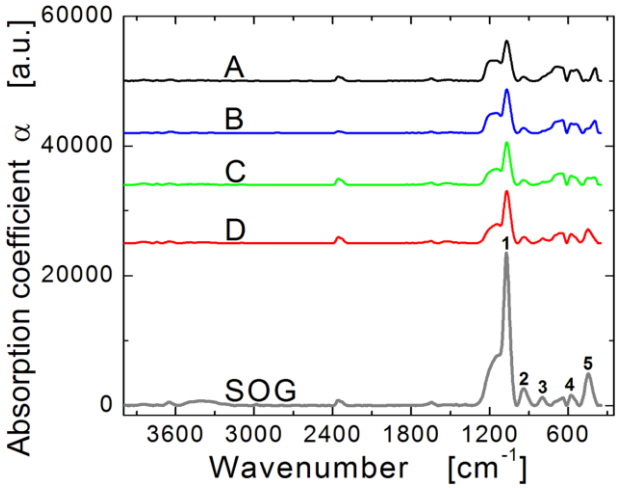

Figure 6. IR spectra (absorbance mode) of TiO_2/SiO_2/glass samples (A-D).

The IR spectra for SOG-based SiO_2 is also included and whose absorption peaks for the Si-O bonds are detected at 1070, 943, 801, 570, and 443 cm^{-1} (peaks 1-5). In order to analyze only the contribution of TiO_2 in the films, the IR spectra of A-D samples must be obtained using only the SOG-based oxide film as reference (SiO_2/glass) at wavenumber between 1600 and 400 cm^{-1} approximately (data in preparation). This way, we are able to eliminate the influence of the highly absorbent peaks related to Si-O bonds (especially those found at 1070 and 443 cm^{-1}).

E. UV-Vis Transmittance Spectroscopy

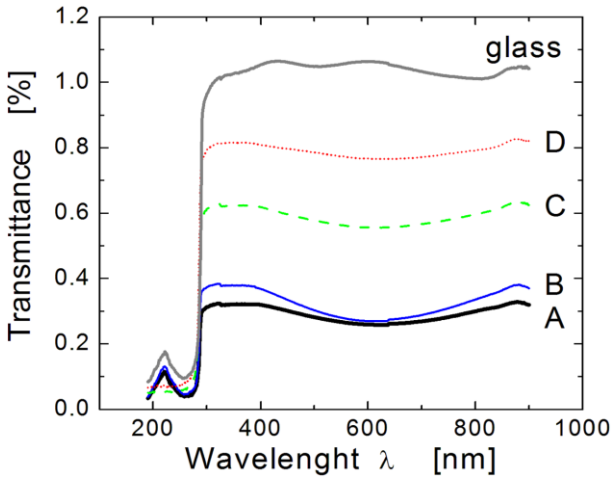

Figure 7. UV-Vis spectra (transmittance) of TiO_2/SiO_2/glass samples (A-D).

Fig. 7 shows the UV-Vis spectra from 190 up to 900 nm region for different np-TiO_2 concentrations (A-D samples), including the spectrum for only the glass substrate. It can be seen that strong absorption occurs at wavelengths λ<290 nm (UV-B regime) for all samples and that transmittance is reduced in direct proportion to the np-TiO_2 concentration as expected. Even though the physical thicknesses for all samples are different (see fig. 4), minimum variations in their optical band gap are expected if we consider different densities for these films. The calculated optical band gap Eg for all A-D samples is at 3.11-3.12 eV. This band gap energy Eg corresponds well with the reported Eg for anatase or rutile TiO_2, between 3.0 and 3.2 eV respectively [15].

F. I-V-Light Characterization

Fig. 8 shows the I-V-Light characteristics of the structure shown previously in fig. 2 (A sample only). Dark, sunlight, sunlight+lamp and UV-B light (~300 nm) conditions were all applied on top of the structures so that surface np-TiO_2 were the first to absorb all possible irradiation coming from these sources. Compared to dark conditions, photogeneration of excess carriers (both electrons and holes) within the TiO_2 nanoparticles is greater after UV-B light exposure and these carriers are directly transferred to both ends of the Al-stripe after applying a low potential difference. During UV-B light irradiation, the total aluminum resistance is reduced by about 43% which represent a moderate change in resistance given by rather low quantum efficiency presented by this structure.

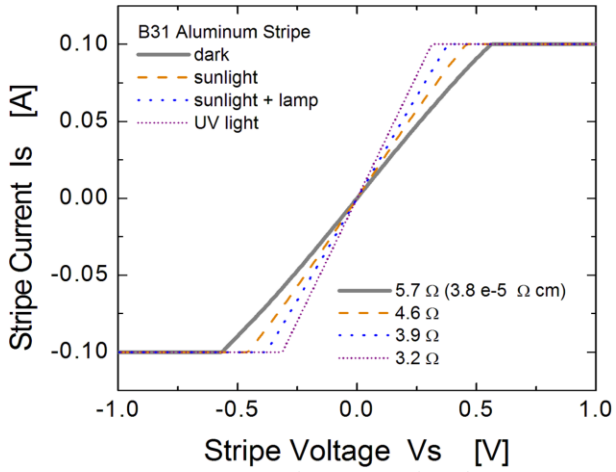

Figure 8. I-V-Light characteristics of Al-stripes before/after light irradiation.

G. Vertical Ti/np-TiO_2/SiO_2/Al/Glass Structure

Previously, I-V-Light characterization for horizontal structures produced a moderate photogeneration of carriers so that the total resistance of an aluminum strip was reduced. However, given that some of the photogenerated carriers will be trapped, recombined or "*lost*" within the SiO_2 matrix or at its interface with np-TiO_2 (any annihilation mechanism), the "*horizontal path*" followed by carriers in the initial structure would reduce their lifetime once they are photogenerated in the np-TiO_2. In order to increase photocarrier lifetime before recombination and thus, increase quantum efficiency during UV-B irradiation, vertical structures are proposed, see fig. 9.

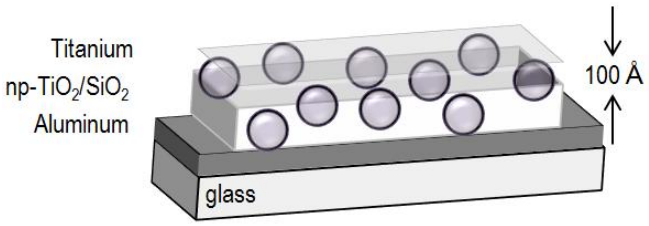

Figure 9. 3D view for a vertical Ti/np-TiO_2/SiO_2/Al/Glass structure where the titanium electrode is 100 Å in thickness, thus being optically transparent.

These vertical structures use Titanium as a gate electrode (only 100 Å in thickness) so that a capacitor in the form of a Metal-Insulator-Metal (MIM) structure is formed. Because of the ultra-thin titanium layer, this gate electrode is highly transparent to all UV-Vis irradiation so that when all carriers are being photogenerated, a vertical transition of these carriers between bottom/top electrodes (by an applied external electric field) would require a shorter distance thus increasing their lifetime before recombination as compared to the horizontal structures. In short, these vertical structures should be able to photogenerate carriers more efficiently and, in contrast with the photoresistor previously described, this MIM structure should be quite similar in function to that of a so-called "photocapacitor" [7-8], where all carriers could be efficiently stored within the dielectric itself right after photogeneration. Thus, a light-driven self-charging capacitor having an efficient storage mechanism of solar energy could

 ISBN: 978-1-61208-297-4

be obtained. The fabrication and testing of this final device is already going on and all results will be soon presented.

IV. CONCLUSIONS

Photocarrier generation during UV-B exposure of rutile-phase np-TiO_2 (embedded within a SiO_2 matrix) in a horizontal np-TiO_2/SiO_2/Al/Glass structure enables a reduction of the total resistance of an aluminum stripe by about 43%. These structures can be fabricated using simple and economic processing techniques, so that immobilization of TiO_2 nanoparticles in a suitable organic matrix for photocarrier generation can be also implemented in vertical Ti/np-TiO_2/SiO_2/Al/Glass MIM structures for more efficient generation of carriers. The vertical structure would act as a photocapacitor, thus enabling direct storage of solar energy.

ACKNOWLEDGMENT

This work was fully supported by the National Council of Science and Technology (CONACyT-Mexico).

REFERENCES

[1] Z. Ding, G.Q. Lu, and P.F Greenfield, "Role of the Crystallite Phase of TiO_2 in Heterogeneous Photocatalysis for Phenol Oxidation In Water", J. Phys. Chem. B, vol. 104, April 2000, pp. 4815-4820.

[2] T.A. Kandiel, R. Dillert, A. Feldhoff, and D. Bahnemann, "Direct Synthesis of Photocatalytically Active Rutile TiO_2 Nanorods Partly Decorated with Anatase Nanoparticles", J. Phys. Chem., vol. 114, February 2010. Pp. 4909-4915.

[3] M.A. Behnajady, N. Modirshahla, M. Shokri, and B. Rad, "Enhancement of photocatalytic activity of TiO_2 nanoparticles by silver doping: photodeposition versus liquid impregnation methods", Global NEST Journal, vol. 10-1, 2008, pp. 1-7.

[4] D.H. Kim, D.K. Choi, S.J. Kim, and K.S. Lee, "The effect of phase type on photocatalytic activity in transition metal doped TiO_2 nanoparticles", Catalysis Communications, vol. 9, March 2008, pp. 654–657.

[5] C.D. Valentin, G. Pacchioni, and A. Selloni, "Origin of the different photoactivity of N-doped anatase and rutile TiO_2", Phys. ReV. B., vol. 70, August 2004, pp. 085116-1, 085116-4 (2004).

[6] O. Diwald, L. Thompson, E.G. Goralski, S.D. Walck, and J.T. Yates, "The Effect of Nitrogen Ion Implantation on the Photoactivity of TiO_2 Rutile Single Crystals", J. Phys. Chem. B, vol. 108, January 2004, pp. 52-57.

[7] T. Miyasaka and T.N. Murakami, "The photocapacitor: An efficient self-charging capacitor for direct storage of solar energy", Appl. Phys. Lett., vol. 85, October 2004, pp. 3932-3934.

[8] C.W. Lo, C. Li, and H. Jiang, "A photoelectrophysical capacitor with direct solar energy harvesting and storage capability", Optical MEMS and Nanophotonics (OPT MEMS), 2010 International Conference on, August 2010, pp. 65-66.

[9] T. Song and B. Sun, "Towards Photo-Rechargeable Textiles Integrating Power Conversion and Energy Storage Functions: Can We Kill Two Birds with One Stone?", ChemSusChem, vol. 6, January 2013, pp.408–410.

[10] X. Zhang, X. Huang, C. Li, and H. Jiang, "Dye-Sensitized Solar Cell with Energy Storage Function through PVDF/ZnO Nanocomposite Counter Electrode", Adv. Mater., June 2013, pp. 1-4.

[11] W. Guo, X. Xue, S. Wang, C. Lin, and Z.L. Wang, "An Integrated Power Pack of Dye-Sensitized Solar Cell and Li Battery Based on Double-Sided TiO_2 Nanotube Arrays", Nano Lett., vol. 12, no. 5, April 2012, pp. 2520–2523.

[12] M.S. Nuckowska, K. Grzejszczyk, P.J. Kulesza, L. Yang, N. Vlachopoulos, L. Häggman, E. Johansson, and A. Hagfeldt, "Integration of solid-state dye-sensitized solar cell with metal oxide charge storage material into photoelectrochemical capacitor", J. of Power Sources, vol. 234, no. 15, July 2013, pp. 91-99.

[13] "Microtrac: Total Solutions in Particle Characterization, NanotracWave", App Note, Microtrac. October 2012, pp. 1-4. http://www.microtrac.com/MTWP/wp-content/uploads/2012/10/Nanotrac-Wave-Temp-Brochure-Ver-9.pdf

[14] J. Tauc, "Optical properties and electronic structure of amorphous Ge and Si", MRS Bulletin, vol. 3, January 1968, pp. 37-46.

[15] J. Dharma and A. Pisal, "Simple method of measurement the band gap energy value of TiO_2 in the powder form using UV/Vis/NIR spectrometer", App Note, Perkin-Elmer Inc. January 2009, pp. 1-4.

 ISBN: 978-1-61208-297-4